NEARSHORE WAVE DAMPING DUE TO THE EFFECT ON WINDS IN RESPONSE TO OFFSHORE WIND FARMS

Ruben R. Gandara[1] and John M. Harris[2]

Despite the progress that has been made in modeling wind wake interaction between turbines in offshore wind farms, only a handful of studies have quantified the impact of wind turbines or wave farms upon surface waves, and there are even less articles about the wave blockage induced by the whole array of turbines upon wind waves. This hypothetical case study proposes a methodology that takes into account the combined effect of wind wake and wave blockage on wind waves when transforming offshore waves to nearshore in an offshore wind farm scenario.

Keywords: offshore wind farm; wind wake modelling; wave blockage modelling; wind farm footprint.

1 MOTIVATION

The wind provides a rich energy source, which can be exploited to achieve a sustainable energy supply for years to come and to meet the increasing demand for energy world-wide. The recent construction of large wind farms offshore makes the implementation of wind energy highly realizable. In addition, energy production increases because larger turbines can be deployed offshore. Current offshore wind farms are often installed in near-shore areas where water depths are less than 20 m and where connection to the electrical grid is convenient.

One of the most important environmental issues associated with offshore wind turbines (along with the visual impact and, to a lesser extent, ambient noise levels) is that the supporting structures are likely to affect the wave and circulation regime, as well as sediment transport, due to the blockage and scattering of wave energy due to the piles. In addition, the activity induced by the rotating blades generates a downwind turbulent wake, within which the wind speeds are lower than the far field (i.e free stream) value. This is likely to have an impact on locally generated wind waves, both within and downwind of the wind farm.

Only a few published studies analyse the impact of wind turbines or offshore wave farms upon surface waves near the coast (CEFAS, 2005; Millar, Smith, and Reeve, 2007). The former investigates the wave blockage effect induced by wind turbines upon surface waves by means of a wave agitation model based on the mild slope equation. The latter estimates the changes in the shoreline wave climate associated with the development of arrays of wave energy converters (WECs) by making use of the SWAN wave transformation model (Booij et al., 1999), along with a set of empirical transmission percentages in order to represent the wave energy damping.

Regarding the wind wake, there is a wide range of publications discussing the modelling of either the vertical wind profile (Lange, Larsen, Højstrup and Barthelmie, 2002) or the wake development *at hub height* downwind of the wind farm (Barthelmie, Pryor, Frandsen and Larsen, 2004).

However, no studies are published that assess the importance of the whole array of wind turbines upon wind waves when considering the effects of wind wake and wave blockage together. The purpose of this study is to quantify the effect of these structures on wind waves, which propagate toward the coast. The main aim is to establish a methodology to establish how much these structures will absorb and scatter wave energy, as well as to quantify the effect of wind speed decay on waves propagating towards the coast.

2 LOCATION AND PROPOSED LAYOUT

This case study considers a *hypothetical* wind farm located 12 km offshore of the Corpus Christi Bay, Gulf of Mexico, U.S. (Figure 1, left). The geographic coordinates are [Lat, Long] = [27.912º, -96.833º]. The choice of a location offshore of the U.S. coast was based on the following factors:

- The U.S. wind industry is a growing market. It represents more than 20% of the world's installed wind power.
- The U.S. does not yet have any offshore wind project fully developed, but many are planned.
- Early in 2011, the U.S. Departments of Energy and Interior unveiled a coordinated strategic plan pursuing the deployment of 10 gigawatts (GW) of offshore wind capacity by 2020 and 54 GW by 2030[3].

[1] Bsc (Hons), Msc. Hydrodynamics & Metocean Department, HR Wallingford Ltd, OX10 8BA, Oxfordshire, UK.
[2] (M. ASCE) Coasts & Estuaries Department, HR Wallingford Ltd, OX10 8BA, Oxfordshire, UK.
[3] Source: www.awea.org

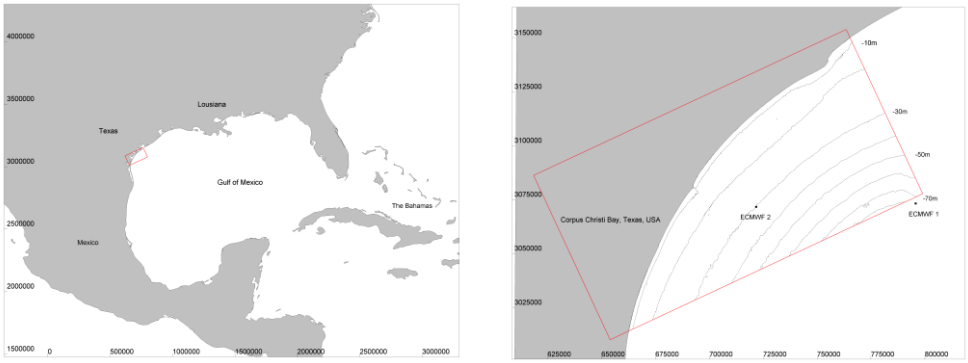

Figure 1. Location of the hypothetical wind farm offshore Corpus Christi Bay (left) and SWAN model domain along with bathymetric contours and ECMWF locations (right).

The main characteristics of the wind turbines considered in the present study are the following:

- 7MW (megawatts), 164 m. blade diameter turbines similar to Vestas V164 7MW model, arranged in a 24 x 18 grid (maximum power generated by the proposed wind farm ≈ 2.7 GW).
- Gravity base with an effective width of 33.5 m.
- Hub height is 120 m. above the sea level.

3 DATA SOURCES

All the geographic datasets and metocean information used in this study are freely available, and were obtained from the following sources:

- Bathymetry and coastline: Coastal Relief Model (NGDC-NOAA)[4]
- Metocean data: ERA-Interim (ECMWF) [5]
- Satellite data: JASON-2 altimeter data (GLOBWAVE)[6]

4 NUMERICAL MODELS

The list of numerical models used in the present study is as follows:

- SWAN (TU Delft): Used to transform offshore waves to nearshore.
- ARTEMIS (Électricité de France - EDF): Wave agitation model based on the mild slope equation. This model is part of the TELEMAC modelling system, and was used to assess the scattered wave energy due to the turbine piles.
- WaSP (Risø DTU) + in-house development: Used to model the wind wake, both within and downwind of the wind farm.

Figure 2 presents a flow chart of the different models and data sources used in the present case study.

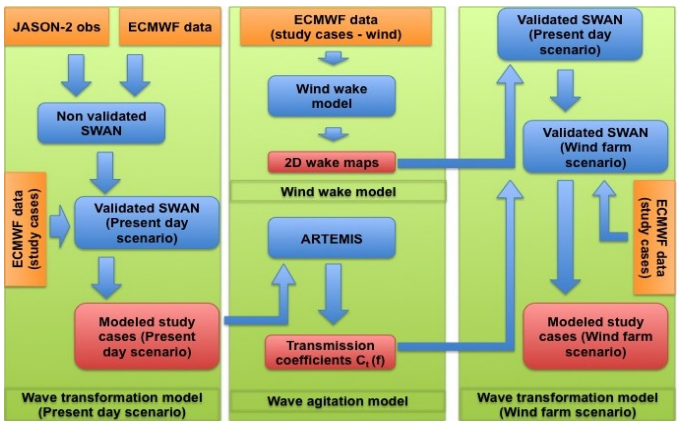

Figure 2. Flow chart of the different models and data sources.

[4] Source: www.ngdc.noaa.gov
[5] Source: www.ecmwf.int
[6] Source: www.globwave.org

5 WAVE TRANSFORMATION MODEL – PRESENT DAY SCENARIO

5.1 Model set up

The Simulating Waves Nearshore (SWAN) model is used to transform offshore waves to nearshore. SWAN is a third-generation phase averaged spectral wave model developed at the Delft University of Technology, the Netherlands (Booij, Ris, and Holthuijsen, 1999). In SWAN, waves are described with a two-dimensional wave action density spectrum, whereas the time-evolution of the action density, N, as the seastate develops, is governed by the time-dependent wave action balance equation.

The overall SWAN grid covers an area of 160 x 84 km., with a grid resolution of 50 m. (Figure 1, right). The digital terrain model (DTM) is based on the data available at the National Geophysical Data Center's (NGDC) 3 arc-second U.S. Coastal Relief Model (CRM), which integrates offshore bathymetry with land topography. Bathymetric data sources include the U.S. National Ocean Service Hydrographic Database, the U.S. Geological Survey (USGS), the Monterey Bay Aquarium Research Institute, the U.S. Army Corps of Engineers, and various other academic institutions. Topographic data are from the USGS and the Shuttle Radar Topography Mission (SRTM). Volumes 3 through 5 also use bathymetric contours from the International Bathymetric Chart of the Caribbean Sea and the Gulf of Mexico project. The vertical datum of the model is Chart Datum (CD).

5.2 Model validation

In this study, the SWAN model is forced with reanalysis data obtained from the ERA-Interim atmospheric model, archived at the European Centre for Medium-Range Weather Forecasts (ECMWF). The model resolution is 0.75°, and the time series span from January 1979 to December 2011. Two ERA-Interim points were considered in the validation step: ECMWF-1 and ECMWF-2, with geographic coordinates [27.75º, 264º] and [27.75º, 263.25º] respectively (Figure 1, right). ECMWF-1 is used to force the SWAN model, since it is located right at the model boundary. ECMWF-2 is used as a control point for check purposes (validation of both the ERA-Interim model itself and the local SWAN model).

No relevant measured buoy wave data were available so as to validate the model. Nevertheless, satellite altimeter data from the JASON-2 mission is available at the GlobWave portal. The ESA GlobWave project is a three year initiative funded by the European Space Agency, and subsidised by CNES, looking to service the needs of satellite wave product users across the globe. JASON-2/OSTM takes over and continues the TOPEX/POSEIDON and JASON-1 missions in 2008, in the frame of a collaboration between CNES, EUMESAT, NASA and NOAA. JASON-2 is equipped with the next generation of POSEIDON altimeter, with an accuracy of about 2.5 cm.

Although JASON-2 is very precise, its spatial resolution is limited. The gap between adjacent ground tracks is a few tens of km., which is a problem for observing small-scale phenomena, particularly those taking place close to the shoreline. The orbit's repeat cycle is just under 10 days, with a ground scanning velocity of 5.8 km/s. This cycle is a trade-off between spatial and temporal resolution designed for the study of large-scale ocean variability.

Figure 3 (left) shows the JASON-2 tracks (black dots) near the study area. The blue dots (circled in red) represent the satellite measurements considered in the validation step. The circle radius is 3km., with its center located on [27.80º, 263.18º]. Only wave measurements registered during 2009 were considered, leading to a total number of 36 events to be simulated. The choice of the specific satellite data is justified as follows:

- The diameter of the circle (6 km.) is roughly the distance covered during a second by the satellite (~5.8 km.)
- The center of the circle was chosen in order to get the maximum number of measured events with good quality (flagged up in the satellite dataset). In addition, the ERA-Interim model resolution is 0.75º, way larger than the distance between point ECMWF-2 and the center of the circle, ~8 km.
- Only wave measurements were considered, since the wind registers were, in general, flagged up as poor quality.

The simulations carried out with SWAN in the validation step were performed considering the following driving parameters:

- Standard JONSWAP wave energy spectrum with $\gamma = 3.3$
- Directional spreading: $\cos^2$
- Third generation mode - Westhuysen - nonlinear saturation-based whitecapping.
- Bottom friction: JONSWAP - 0.038

Figure 3 (right) shows the comparison of the satellite measurements (blue) vs. SWAN results (magenta) at the center of the circle. ERA-Interim points ECMWF-1 (orange) and ECMWF-2 (green) are plotted as well.

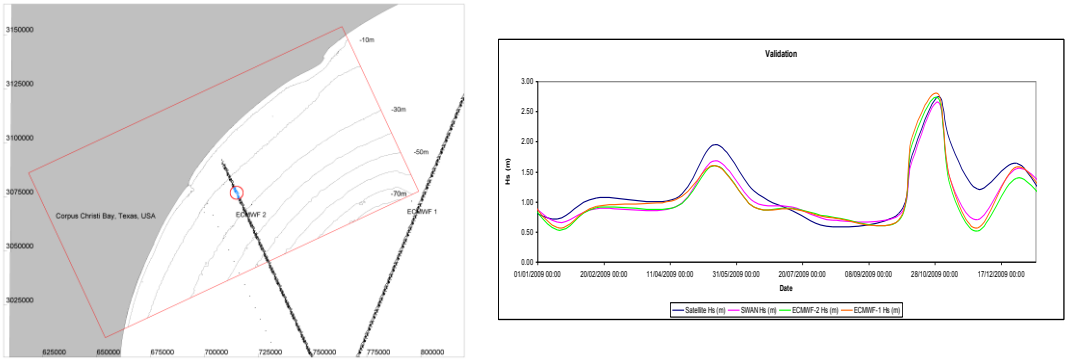

Figure 3. JASON-2 satellite tracks and data considered in the validation step (left). ERA-Interim data and SWAN model results compared vs. satellite measurements (right).

The temporal variability of the measured and modelled significant wave heights are similar at the center of the circle (blue and magenta lines, respectively). For the majority of the modelled events, the SWAN results are slightly lower than the measured values (especially by the end of 2009), but overall, it seems to reproduce the behaviour of the wind waves around the area in a sensible way. ERA-Interim reanalysis model data at location ECMWF-1 and ECMWF-2 show a very similar pattern, both between themselves, measurements and modelled values. In addition, it must be borne in mind that the ERA-Interim model grid is much coarser than the altimeter resolution, which tends to smooth the results. Consequently, it was considered that the ECMWF data and the driving parameters set up in SWAN were suitable to initialise the wave model.

5.3 Study cases

The principal marine environmental input to the metocean analysis in this study is the wind speed, since the performance of the turbines and therefore the different operational conditions are related to this variable. Table 1 presents the U_{10} wind speed information in the ECMWF-1 dataset. The $U_{50\%}$, $U_{90\%}$ and $U_{99\%}$ columns show, for each of the 22.5º sectors, the U_{10} value that is not exceeded for that percentage of the total time. Regarding directional sectors, two directions were considered so as to test the sensitivity of the model to the wind/wave direction: SSE, as it is the most frequent sector (~21% of occurrence), and E, since it is the direction most misaligned with the normal to the proposed wind farm layout (the layout will be introduced later in Section 6).

Table 1. U_{10} frequency table at point ECMWF-1

Sector	Number of observations	Probability (%)	$U_{50\%}$ (m/s)	$U_{90\%}$ (m/s)	$U_{99\%}$ (m/s)
N	2805	5.82	8.43	12.77	15.52
NNE	3180	6.60	7.58	11.47	14.22
NE	2628	5.45	6.32	9.94	13.06
ENE	2898	6.01	5.57	8.98	12.61
E	2773	5.75	5.38	8.53	12.03
ESE	3912	8.11	5.44	8.37	11.33
SE	6720	13.94	6.27	9.14	11.56
SSE	10058	20.86	7.01	10.14	12.70
S	6540	13.57	6.93	10.49	13.33
SSW	2264	4.70	5.57	9.18	12.01
SW	802	1.66	4.12	7.44	10.56
WSW	451	0.94	3.69	6.50	9.02
W	357	0.74	3.39	7.19	10.26
WNW	461	0.96	4.39	9.60	13.97
NW	849	1.76	6.57	12.35	15.71
NNW	1514	3.14	7.94	12.75	15.75

For each of the two wind sectors considered, three wind conditions were tested:

- The strength of the wake from the turbines depends on the axial thrust force coefficient, which controls the strength of the wake: as the wind speed increases towards the cut-off point, the thrust coefficient steadily decreases. Consequently, the effect of the wind farm upon the ambient wind regime at higher wind speeds is substantially reduced, because the resistance of the turbines is correspondingly less.
  However, the wind speed that will give the strongest or most persistent wake is defined as the one corresponding to the highest possible wind speed that can occur at the peak thrust coefficient. This is denoted as the *critical* case.
  On that basis, a wind speed at hub height of 9 m/s was taken for the critical case, giving about 7.5 m/s at 10m above Mean Sea Level (MSL), with a hub height taken as 120 m. The relationship between wind speeds at turbine hub height and at 10 m above MSL is derived using the implicit solution recommended in DNV-RP-C205 (2010).
- The limiting wind speed beyond which the turbines are shut down, is 25 m/s at the hub height and with a predicted equivalent U_{10} value of 19.6 m/s.
- An intermediate wind condition equal to the 99% of non-exceedance (12.70 m/s for the SSE sector and 12.13 m/s for the E sector). This denoted as the *99% no exceedance* case.

In order to provide realistic boundary conditions to the wave transformation model, a wave condition must be associated with each of the wind cases considered. The relationship between U_{10} and significant wave height H_s was derived by means of wind speed vs. H_s scatter plots. These scatter plots were produced for each of the wind sectors SSE and E. The wave direction was considered the same as the wind direction in all cases.

When the offshore significant wave heights had been derived, wave period values were associated with each of the wave events. Peak wave period (T_p) values were associated with significant wave heights based on the H_s vs. T_p frequency table populated with the information in the ECMWF-1 time series. Finally, all the cases considered a still water level of MSL (+0.28 m. CD), since this represents an average tidal state.

Table 2 summarises all the metocean parameters of the operational cases that were used as input to the wave transformation model.

Table 2. Study cases

Sector	Case	H_s (m)	T_p (s)	U_{10} (m/s)	Dir (deg N)
SSE	Critical	1.15	8	7.50	157.5
	99% no exc.	1.91	9	12.70	157.5
	Shut down	2.92	10	19.60	157.5
E	Critical	1.13	8	7.50	90.0
	99% no exc.	2.13	9	12.13	90.0
	Shut down	5.00	12	19.60	90.0

For illustrative purposes, H_s and direction vector plots for the critical case for wind sectors SSE and E are shown in Figure 4. Points 1, 2 and 3 are locations where model results have been tabulated.

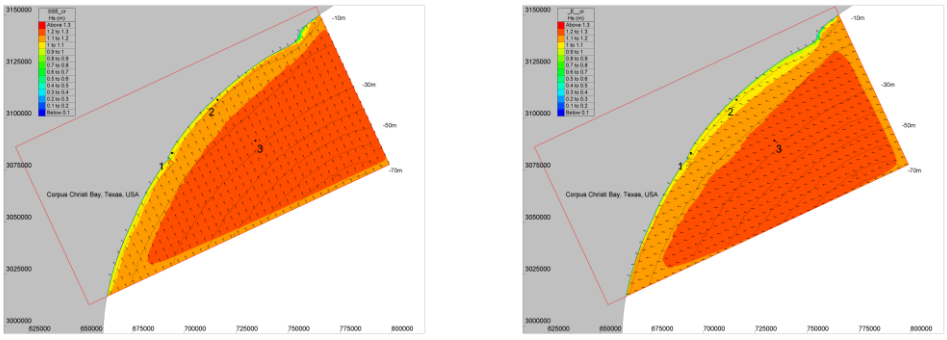

Figure 4. SWAN model results for the present day scenario. H_s and direction vector plots for the critical case. SSE sector (left) and E sector (right).

6 WAVE AGITATION MODEL – PARTIAL WAVE BLOCKAGE

One of the principal types of environmental effect that could be exerted by an offshore wind farm upon the ambient wind and wave regime is direct modification of the local wave climate due to partial blocking effects caused by the presence of the wind turbine foundations. This modification is likely to be more significant under long-term ambient conditions than during a major storm event, because in the former situation, the wavelengths are likely to be shorter relative to the principal diameter of the support structure, thus encouraging the possibility of wave scattering.

With regards to the numerical modeling, and due to the nature of the SWAN model, diffraction is not explicitly modelled. In the literature, there are some references to empirical transmission coefficients (see Millar, Smith and Reeve, 2007 – transmission coefficients for WECs), but there are virtually no references to the quantification of the wave blockage depending on the geometry of the piles, the layout and the local metocean conditions. The present article proposes a quantitative assessment of the wave energy scattering induced by the piles of the turbines, based on the transmission ratio:

$$Transmission\ ratio = \frac{Transmitted\ wave\ energy_{WINDFARM}}{Transmitted\ wave\ energy_{NO\ WINDFARM}} \qquad (1)$$

This transmission ratio can be estimated by making use of a wave agitation model. ARTEMIS, the model adopted in the present study for the prediction of wave scattering and diffraction by the turbine support structures, is part of the TELEMAC finite element hydraulic modelling system. The ARTEMIS model is based on the finite element solution of the Elliptic Mild Slope Equation. It was developed by the National Hydraulics Laboratory (Laboratoire National d'Hydraulique – LNH) of the Research and Development Division of the French Electricity Board, Electricité de France (EDF-DER).

ARTEMIS is a linear finite element model, which is used to calculate wave heights in an area of interest corresponding to a given incident wave condition. ARTEMIS includes the effects of depth refraction and shoaling, diffraction due to the seabed and around surface piercing structures and complete or partial reflections from harbour boundaries. The energy dissipation processes of wave breaking and seabed friction are also included in the model.

Figure 5 shows the extents of the proposed wind farm layout along with the model bathymetry. The separation between turbines is 1700 m. in the X-axis (rows) and 1000 m. in the Y-axis (columns). Unfortunately, the simulation of the whole extent of the wind farm is not feasible, since the computational effort required in order to handle a numerical mesh of more than 10 million nodes is simply prohibitive.

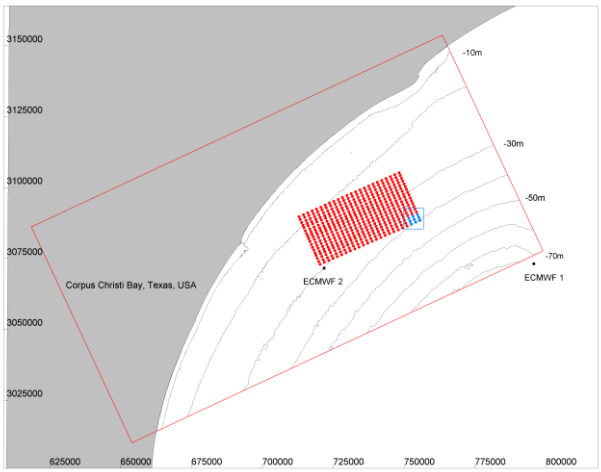

Figure 5. Proposed wind farm layout within the local SWAN model. Wind farm subsection modelled in ARTEMIS is shown in blue.

An optimum compromise between the extents of a representative subsection of the wind farm, the model resolution and the computational performance was achieved by means of a mesh suitable for representing wave periods of 6 s. and above. The mesh resolution is 9 m., with a flat bottom of -28 m. CD. This level is an average depth representative of the wind farm area. Figure 5 shows the subsection of the wind farm considered, where the blue square is the ARTEMIS model boundary.

Figure 6 shows the ARTEMIS model mesh for the wind farm scenario (i.e. with piles in place) along with the control sections used to extract results so as to derive the transmission functions $C_t(f)$.

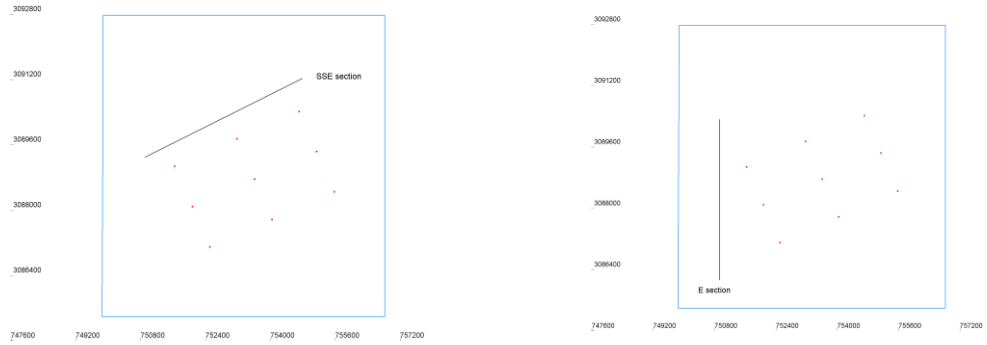

Figure 6. ARTEMIS model for the wind farm scenario. Turbine piles are shown in red. Control sections for SSE conditions (left) and E conditions (right) are shown in black.

Control sections should be aligned not with the downwind row of turbines but with the incoming wind/wave direction. Our experience shows that the wave disturbance pattern downwind of the modelled subsection is poorly captured when the control section is misaligned with the wind/wave direction, leading to errors of up to 10% when calculating C_t values based on frequency dependent expressions (discussed later in the article).

The computation of random sea states in ARTEMIS is based on the principle of linear superposition. That is, it models a random sea state by means of a given number of unidirectional and monochromatic waves depending on the directional spreading and frequency resolution desired, and then combining the results of these monochromatic waves on an energy basis.

Table 3 presents the spectral components of the wave conditions extracted from SWAN at the ARTEMIS boundary (south and east boundaries for the SSE and E conditions, respectively). ARTEMIS decomposes the input wave spectrum (assuming a JONSWAP spectral shape) on an energy basis: it splits the spectrum in equal energy bins, with the number of bins (i.e. monochromatic waves) equal to the number of periods specified by the user in order to resolve the energy spectrum.

Table 3. ARTEMIS wave agitation model - components

Tp (s)	T component	T (s)	H_s SSE (m)	H_s E (m)	m0 SSE (m^2/Hz)	m0 E (m^2/Hz)	H_s comp SSE (m)	H_s comp E (m)
8	T1	4.8	1.29	1.28	0.02080	0.02048	0.58	0.57
	T2	6.7			0.02080	0.02048	0.58	0.57
	T3	7.6			0.02080	0.02048	0.58	0.57
	T4	8.1			0.02080	0.02048	0.58	0.57
	T5	9.0			0.02080	0.02048	0.58	0.57
9	T1	5.4	2.45	2.51	0.07503	0.07875	1.10	1.12
	T2	7.5			0.07503	0.07875	1.10	1.12
	T3	8.5			0.07503	0.07875	1.10	1.12
	T4	9.1			0.07503	0.07875	1.10	1.12
	T5	10.1			0.07503	0.07875	1.10	1.12
10	T1	6.0	4.36	-	0.23762	-	1.95	-
	T2	8.3			0.23762	-	1.95	-
	T3	9.5			0.23762	-	1.95	-
	T4	10.1			0.23762	-	1.95	-
	T5	11.2			0.23762	-	1.95	-
12	T1	7.2	-	5.8	-	0.42050	-	2.59
	T2	10.0			-	0.42050	-	2.59
	T3	11.4			-	0.42050	-	2.59
	T4	12.1			-	0.42050	-	2.59
	T5	13.5			-	0.42050	-	2.59

Nevertheless, this range of periods is insufficient to solve the spectral components associated with the lowest spectral period components in the study cases listed in Table 3. Due to this restriction, the following strategy was adopted so as to estimate the C_t values dependent on wave frequency:

- Initially, and for both the baseline and the wind farm scenarios, multidirectional (i.e defining 5 wave directions per wave period so as to simulate the directional spreading) monochromatic waves with mean periods of 6 and 11.2 s. for the SSE sector, and 6 and 13.5 s. for the E sector were run. Figure 7 shows the JONSWAP wave energy spectral curves for the critical, 99% no exceedance and shut down cases in magenta, blue and green respectively. The magenta and green vertical lines indicate the maximum and minimum spectral frequency components. The vertical red line indicates the maximum frequency (or minimum period) computed by the wave agitation model, therefore ARTEMIS will not reproduce the effect of frequencies higher than this value.

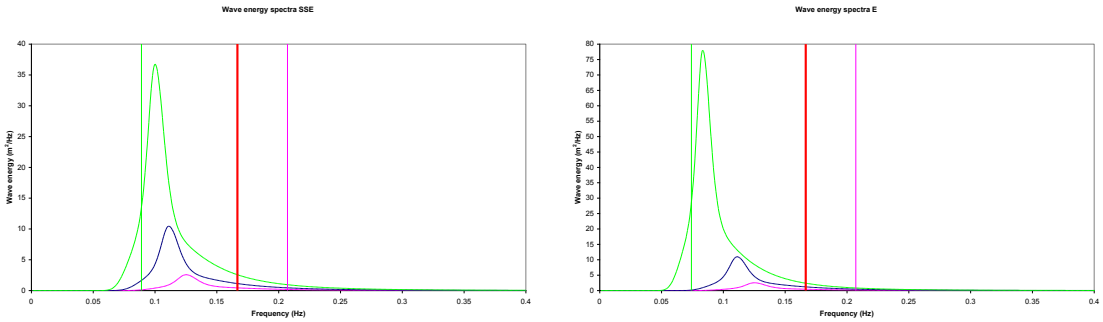

Figure 7. JONSWAP wave energy spectral curves for the study cases. SSE sector (left) and E sector (right).

- For both sectors, the former value represents the lowest wave period that can be simulated with the mesh, whereas the latter is the maximum spectral component in the longest peak period to be run. Figure 8 shows the ARTEMIS model results for the critical case from East, for both the baseline and wind farm scenarios.

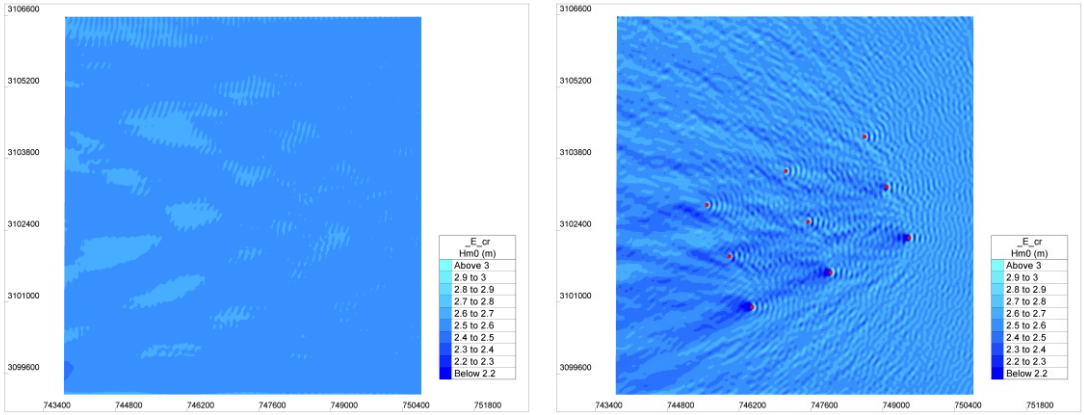

Figure 8. ARTEMIS H_{m0} model results for the critical case from E run in multidirectional / monochromatic mode. Present day scenario (left) and wind farm scenario (right). Piles in the wind farm scenario shown in red.

- Based on the average values of H_s along the relevant control sections, transmission ratios were obtained using Eq (1). Table 4 presents these coefficients.

Table 4.- Transmission ratios for the multidireccional/monochromatic runs

T	Sector	
(s)	SSE	E
6	98.00%	97.80%
11.2	99.15%	-
13.5	-	97.70%

- Figure 9 shows the linear $C_t(f)$ functions obtained from the data in Table 4.

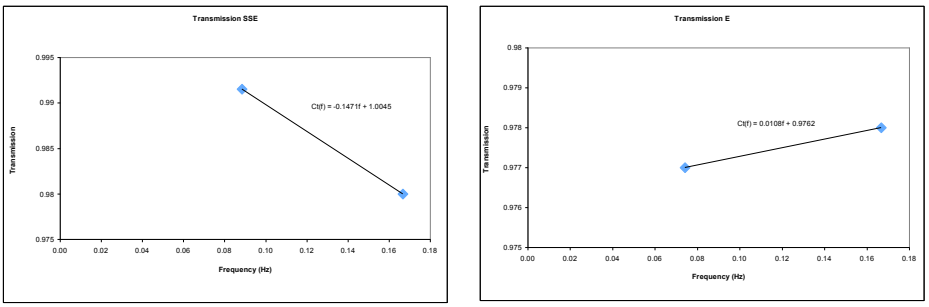

Figure 9. Linear $C_t(f)$ functions derived from the multidirectional and monochromatic runs. SSE sector (left) and E sector (right).

The literature states that the diffraction/reflection effects due to piles are significant when the ratio given by the pile diameter over the wavelength is either > 0.2 or 0.1, depending on the author. According to Figure 9, it seems that this is consistent with SSE conditions, whereas for the E conditions it is the opposite.

Further tests considering each of the spectral components of the shut down cases listed in Table 3 confirmed the trends shown in Figure 9. The discrepancy with the theory can be explained this way: the length of the E control section is not long (or short) enough so as to capture the wave diffraction pattern, which becomes more complicated when the incoming wind/wave direction is misaligned with the normal to the modelled wind farm subsection. In this case, a tuning exercise based on the length of the control section is required in order to obtain precise transmission ratios.

Table 5 shows the linear expressions of $C_t(f)$ for the different sectors, obtained from Table 4 and Figure 9.

Table 5. C_t as function of frequency (Hz)

Sector	$C_t(f)$
SSE	$C_t(f) = -0.1471f + 1.0045$
E	$C_t(f) = +0.0108f + 0.9762$

As validation of the estimation of the random wave transmission coefficients presented in Table 5, the critical and shut down cases shown in Table 3 were run in multidirectional random mode (i.e. 5 periods and 5 directions) in ARTEMIS. The 99% no exceedance cases were not simulated, since all its frequency components lay within the frequencies simulated in the other two cases. Wave period components below 6 seconds cannot be resolved with the current ARTEMIS mesh, and therefore they were truncated to this minimum value. As it can be seen from Table 3, this affects the critical case from SSE only.

Once the transmission ratios for the multidirectional random wave conditions were obtained using Eq. (1), these were compared to the equivalent values obtained making use of the expressions in Table 5. To do so, each frequency component of a JONSWAP wave energy spectrum S(f), as defined by Goda in 1985, was scaled by the appropriate $C_t(f)$ so as to calculate an overall integrated transmission coefficient for the random wave following Eq. (2):

$$Transmission\ ratio = \frac{\int_0^\infty S(f) \cdot C_t(f) \cdot df}{\int_0^\infty S(f) \cdot df} \qquad (2)$$

It must be noted that the $C_t(f)$ expressions in Table 5 can lead to values either lower than 0 or greater than 1, depending on the frequency considered. Since this is not physically possible, we need to restrict the outcome from these expressions following Eq. (3):

$$C_t(f) = f(x) = \begin{cases} 1, & C_t(f) > 1 \\ C_t(f), & 0 \le C_t(f) \le 1 \\ 0, & C_t(f) < 0 \end{cases} \qquad (3)$$

Table 6 shows the transmission ratios obtained in the validation step, both directly from the model using Eq. (1) and from the equivalent scaled JONSWAP spectrum using Eq. (2).

Table 6. Validation of the derived expressions for $C_t(f)$

Sector	Source	Tp (s)		
		8	10	12
SSE	From model	98.40%	98.58%	-
	Empirical	98.25%	98.69%	-
E	From model	98.50%	-	98.90%
	Empirical	97.78%	-	97.73%

It can be seen from Table 6 that the comparison between the different methods for sector SSE is strikingly good, with differences kept under 0.15%. For the E sector, where the incoming wind/wave direction is misaligned with the normal to the wind farm, the mismatch between the two methodologies goes up to 1.17%. This relatively large difference states the need for a tuning exercise for the control sector considered in the wave agitation model under easterly conditions.

Table 7 shows the summary of the transmission ratios obtained for each direction sector and wave condition, for a 3 x 3 turbines wind farm subsection.

Table 7. Transmission coefficients Ct

Sector	Critical	99% no exc.	Shut down
SSE	0.9825	0.9850	0.9869
E	0.9778	0.9776	0.9773

7 WIND WAKE MODELLING

The turbines in a wind farm generate a downwind turbulent wake, within which the wind speeds are lower than the far-field value. In order to get a better picture of this effect, this section presents a short briefing on the characteristics of the Horns Rev 1 wind farm, which is located in the North Sea, between 14 and 20 km. west of Esbjerg in Denmark. It has been the subject of several years' research into power output and wind-wake generation (at hub height), much of which has been published by the Danish wind energy research community.

Observations of the wake from Horns Rev 1 offshore wind farm, made using the ERS-2 satellite equipped with a synthetic aperture radar, show that the influence of the wind farm upon the sea surface can extend many kilometres down wind, under certain atmospheric conditions. Figure 10 shows an observed wake from Horns Rev 1, with the wind coming from 110° - the length of the wake is at least 0.4° of longitude. In the figure, the wind is blowing along the principal diagonal of the wind farm footprint, which is one of the most severe cases for the strength of the downwind wake.

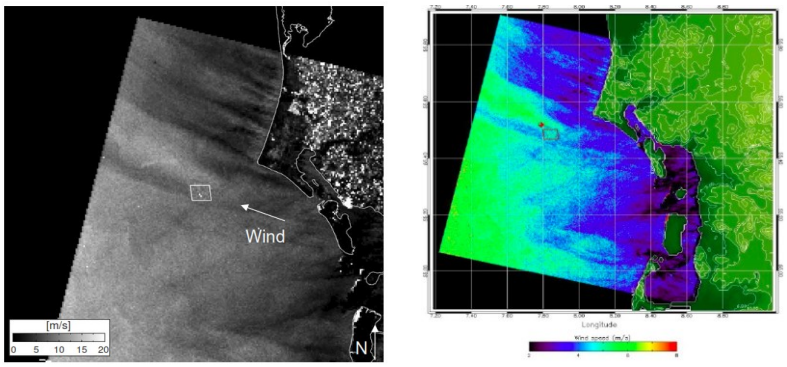

Figure 10. Wind speed map over Horns Rev wind farm observed by the ERS-2 satellite and detected using synthetic aperture radar (SAR). Source: Christiansen and Hasager (2005b, left and 2007, right). The outline parallelogram represents the boundary of the Horns Rev wind farm array.

Analysis of synthetic aperture radar gathered by the ERS-2 satellite for Horns Rev 1 offshore wind farm, indicates a downwind wake persistence length of at least 20 km *at sea level*. Figure 11 shows the velocity deficit within and downwind Horns Rev 1.The vertical line in Figure 11 denotes the maximum wind farm boundary position and the wind is blowing from left to right, where the upwind edge is at a

distance of zero km. The figure shows that the velocity deficity (that is the reduction in wind speed as a proportion of the far field ambient value) *at sea level* achieves a maximum value at about 5 km downwind of the wind farm footprint – as opposed to within the footprint itself. This is due to interaction between the individual wakes of the wind turbines; the wakes need to travel a certain distance down-wind before they can make contact with the sea surface. The maximum value of velocity deficit is about 10-11% in this example – that is, the minimum wind speed down-wind of the wind farm *at sea level* is about 90% of the free stream value. Higher velocity deficits than this have also been reported in the literature.

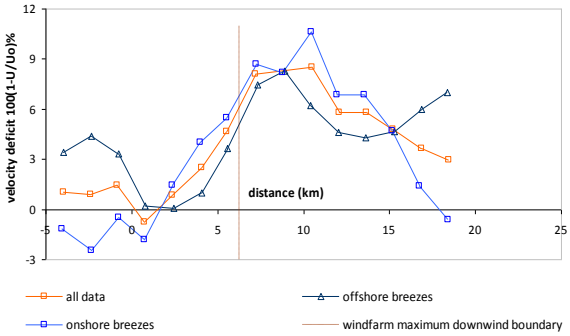

Figure 11. Average velocity deficit obtained from a total of 19 satellite SAR wind maps.

The question we would now ask is that for the large offshore wind farms currently being planned, what is their effect likely to be upon the local wind-wave climate, and what will be the resultant influence upon the transport of sediment around the affected coastlines? Will they exert any influence upon the inshore sediment budget, and will this be positive or negative from the viewpoint of sustainability of the coastline?

We have developed a numerical model for predicting the turbine wake interaction at any elevation within and downwind of an offshore wind farm. The model generates a prediction of the wind speeds at a given elevation, onto a 2D map, which can then be used in a regional wave model, to develop the influence upon the local nearshore wave climate. In Figure 12, we compare the predictions of wind speed deficits observed at Horns Rev 1, obtained using our wake model, with the observed values, for all of the synthetic aperture radar data reported by Christiansen and Hasager (2005b). The level of agreement between the numerical model and the observations is highly encouraging.

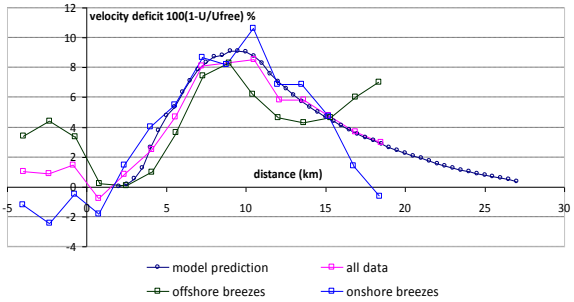

Figure 12. Comparison between the velocity deficits in the ERS-2 synthetic aperture radar observations and those predicted by the wake interaction model, applied to Horns Rev.

The model that we have developed is of the geometric type, fitting into the same family as WaSP (Risø, Denmark), Windfarmer (GL-Garrad-Hassan, UK), and WindPro (EMD, Denmark). In this type of solution, the wakes from each of the individual wind turbines are predicted in 3D space and their interactions with each other are predicted using accepted empirical solutions. As the wind moves through the array from the upwind to the downwind side, there is a gradual reduction in wind speed within the wind farm footprint; the wind then eventually recovers to the ambient level, at some distance downwind of the wind farm, where the velocity deficit tends to zero, and the wind speed tends back towards the free stream value, as Figure 12 suggests.

None of the standard wind farm packages provides a means of satifactorily predicting the wake of the wind farm downwind on a plane at or near to sea level, in a manner that agrees with observations;

the new work that we have undertaken has been to develop a calibrated model for making such a prediction.

Within the wind farm itself, we have used WaSP to predict the wind speeds immediately down wind of the turbines, at turbine hub height. We subsequently use our own numerical model, for predicting the wind speed and the wake due to the wind farm array, at an arbitrary elevation just above sea level. Our model uses a calibrateable version of the N.O Jensen wake format. We summate the contributions from individual interacting wakes at any point by using the same method as that used in WaSP, which is a root sum square approach. The calibration factor introduced into the N.O Jensen wake formulation enables us to control the rate of rise and decay of the velocity deficit downwind of the array on a horizontal plane at any elevation, so that we are able to reproduce the values observed by Christiansen and Hasager (2005) at sea level.

2D wind speed maps were generated for each of the study cases, considering the wind turbine characteristics listed in Section 2 in the present article. These maps were later used as input to the SWAN model so as to represent the wind farm scenario, in combination with transmissive obstacles that reproduce the partial wave blockage.

For illustration purposes, Figure 13 shows the difference in U_{10} 2D maps, between the baseline and wind farm scenarios, for the critical wind speed case for sectors SSE and E. No waves or transmissive obstacles are taken into account. As it can be seen from the figure, our model is able to realistically simulate the wind wake downwind the wind farm area. The wake extends to the shoreline in both cases.

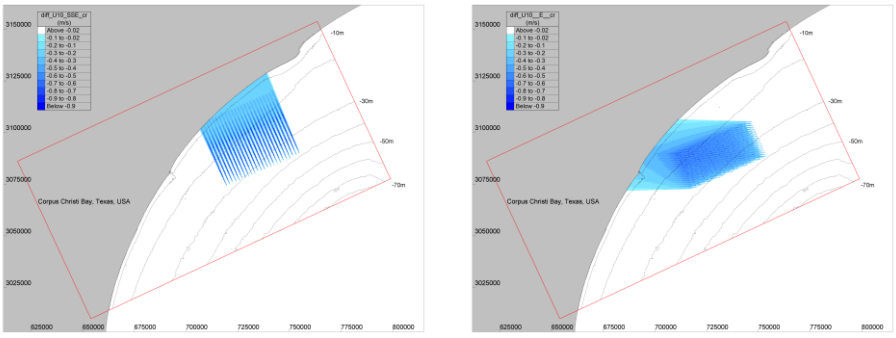

Figure 13. 2D U_{10} difference maps (wind farm scenario minus present day scenario). Critical case from SSE (left) and E (right).

8 WAVE TRANSFORMATION MODEL – WIND FARM SCENARIO

Once the transmission coefficients introduced in Section 6 and the 2D wind wake maps described in Section 7 were obtained, the baseline wave transformation model presented in Section 5 was updated to include the effect of the foundations within the proposed wind farm area. The proposed wind farm layout shown in Figure 5 was re-grouped in multiple 3 x 3 turbine blocks, as described in Sections 5 and 6. Straight lines (see Figure 6) with a suitable associated Ct value (see Table 7) were then included in the SWAN model. Each of these lines represents a 3 x 3 turbines block equivalent to the one shown in blue in Figure 5. This way the wind farm layout was discretised and represented in the wave transformation model.

The six study cases listed in Table 2 were simulated with the SWAN model updated with their corresponding obstacles and C_t values. The wind wake maps reported in Section 7 were used to specify the wind field boundary conditions over the model grid. In this way, the combined effect of wave blockage and wind wake induced by the wind farm was simulated in the wave transformation model.

As an example, significant wave height H_s and direction vectors plots for the critical case for wind directions SSE and E are shown in Figure 14.

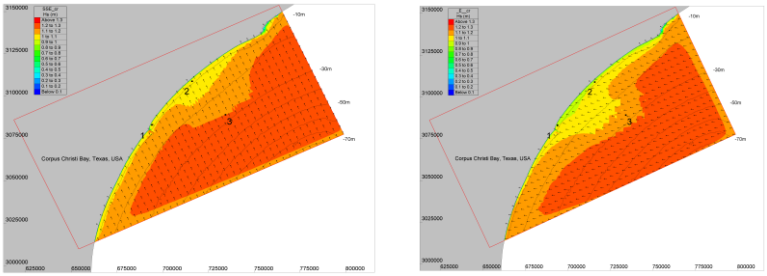

Figure 14. SWAN model results for the wind farm scenario. H_s and direction vector plots for the critical case. SSE sector (left) and E sector (right).

For illustration purposes of the effect of the wind wake and pile blockage on waves, figures 15, 16 and 17 show, for the critical case, the H_s difference plots for the following cases:

- Difference in Hs between the wind farm scenario (associated 2D wake map and transmissive obstacles considered) and the baseline scenario.
- Difference in Hs between the wind farm scenario (associated 2D wake map considered only – no transmissive obstacles) and the baseline scenario.
- Difference in Hs between the wind farm scenario (associated transmissive obstacles considered only – no 2D wake map, but with the free stream wind field) and the baseline scenario.

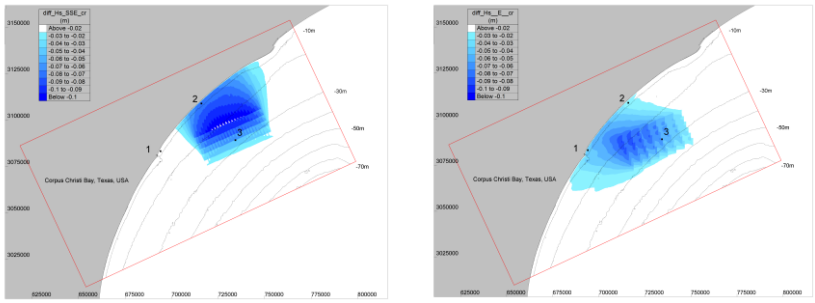

Figure 15. Difference in Hs for the critical case. Both wind wake and wave blockage considered in the wind farm scenario. SSE sector (left) and E sector (right).

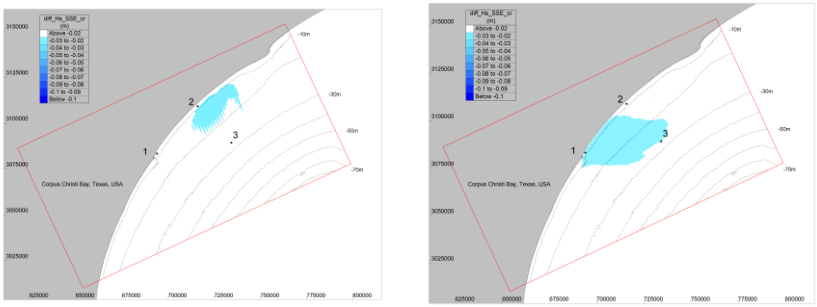

Figure 16. Difference in Hs for the critical case. Only wind wake considered in the wind farm scenario. SSE sector (left) and E sector (right).

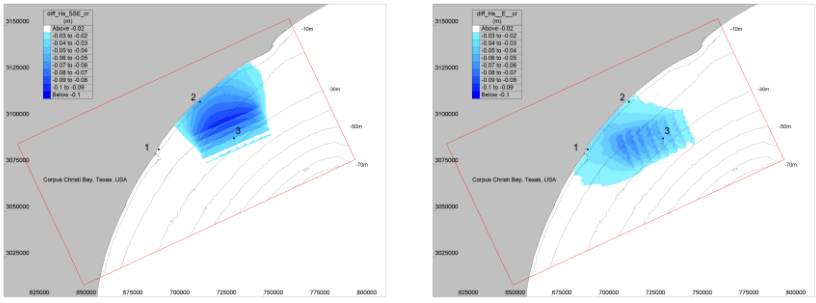

Figure 17. Difference in Hs for the critical case. Only wave blockage considered in the wind farm scenario. SSE sector (left) and E sector (right).

Table 8 shows the UTM coordinates of the tabulation points where model data was extracted.

Table 8. Tabulation points

Point	X - UTM 14N	Y - UTM 14N
1	694027	3083172
2	716024	3108876
3	734275	3089140

Table 9 presents the tabulated results for the different scenarios, including the alternative ones considering only the effect of either the wave blockage or the wind wake.

Table 9. Tabulated Hs values for the different scenarios

Sector	Case	Point	Present day	Development (Wind wake + wave blockage)	Development (Only wind wake)	Development (Only wave blockage)
			H_s (m)	H_s (m)	H_s (m)	H_s (m)
SSE	Critical	1	1.03	1.03	1.03	1.03
		2	1.09	1.02	1.07	1.04
		3	1.26	1.22	1.25	1.22
	99% no exceedance	1	2.05	2.05	2.05	2.05
		2	2.25	2.15	2.23	2.17
		3	2.46	2.40	2.45	2.40
	Shut down	1	2.60	2.60	2.60	2.60
		2	3.23	3.21	3.23	3.21
		3	4.47	4.39	4.47	4.39
E	Critical	1	1.05	0.98	1.02	1.01
		2	1.02	0.99	1.02	1.00
		3	1.24	1.14	1.22	1.16
	99% no exceedance	1	2.08	2.00	2.07	2.02
		2	2.05	1.99	2.04	2.00
		3	2.47	2.28	2.45	2.31
	Shut down	1	2.75	2.74	2.75	2.74
		2	3.30	3.29	3.30	3.29
		3	5.74	5.35	5.73	5.36

Table 9 shows that the wave blockage is more severe than the wind wake effect on waves. As expected, tabulation point 1 shows greater differences in H_s when winds are blowing from E, whereas point 2 suffers from a more severe impact when winds blow from SSE. At point 3, placed in the middle of the wind farm, waves show greater differences when winds are blowing from E, since waves have to travel through a larger number of turbines than when winds blow from E. Relative differences in H_s between the wind farm (considering the combined effect of the wind wake and wave blockage) and the baseline scenarios reach up to 6.73% at point 1 (E sector), 6.76% at point 2 (SSE sector) and 8.52% at point 3 (E sector).

9 SUMMARY AND CONCLUSIONS

In scientific literature, only a few studies analyse the impact of wind turbines or wind farms upon surface waves near the coast. In these cases, the wave energy damping caused by the structures is usually modelled by means of empirical transmission percentages. The authors of the present article have identified a lack of studies assessing the combined effect of wind wake and wave blockage induced by offshore wind farms.

The wind farm footprint, combined with the partial wave blockage induced by the turbine

foundations has an effect on locally generated wind waves and potentially upon nearshore sediment dynamics when acting over a long period of time. The hypothetical case study presented here proposes a methodology to address this combined effect. An in-house model has been developed to enhance the capabilities of the existing standard wind farm packages, being able to reproduce the evolution of the wind wake downwind of the wind farm.

The methodology presented to describe the blocking effect of piles on waves as a function of the frequencies of the wave energy spectrum seems accurate when dealing with winds/waves aligned with any of the normal directions to the wind farm. Non-aligned waves are likely to be scattered wider, making it difficult to capture the complete interference pattern and leading to inaccurate expressions for transmission coefficient $C_t(f)$. In that case, a tuning exercise based on the length of the control section is required in order to obtain precise transmission ratios.

In addition, this way of deriving the transmission coefficients is extremely useful when the number of cases required to be tested in a detailed study of a wind farm is large, reducing the amount of runs needed to define accurately the wave blockage.

10 ACKNOWLEDGMENTS

The authors would like to thank Dr. Richard Swift for his guidance, critical feedback and technical contribution to this article.

11 REFERENCES

Alari, V. and Raudsepp, U., 2012, 'Simulation of Wave Damping Near Coast due to Offshore Wind Farms'. *Journal of Coastal Research: Volume 28, Issue 1*: pp. 143 – 148.

Barthelmie, R.J., Pryor, S.C., Frandsen,S. & Larsen, S, 2004. 'Analytical and empirical modelling of flow downwind of large wind farm clusters'. *In Special Topic Conference: The science of making torque from wind*, Delft (NL), pp. 292-303.

Booij, N., Ris, R.C., and Holthuijsen, L.H., 1999. 'A Third-Generation wave model for coastal regions. Model description and validation'. *Journal of Geophysical Research*, C104, 7649–7666.

Christiansen, M.B. and Hasager, C.B. (2005a): Wake effects of large offshore wind farms identified from satellite SAR. *Remote Sensing of Environment* (2005), **98**, 251-268.

Christiansen, M. B., Hasager, C. B. (2005b). 'Wake studies around a large offshore wind farm using satellite and airborne SAR'. Skt. Petersburg, Russia, 20-24 June 2005. 31st *International Symposium on Remote Sensing of Environment (ISRSE)*. Same issue.

Coastal Engineering Manual, 2003. Part VI, Chapter 5, pp. 242–245, Vicksburg, Mississippi: U.S. Army Corps of Engineers.

CEFAS (Centre for Environment, Fisheries, and Aquaculture Science), 2005. 'Assessment of the changes to the inshore wave regime as a consequence of an offshore wind array', *project AE1227*. Lowestoft, UK.

DET NORSKE VERITAS AS. 'Design of Offshore Wind Turbine Structures', *Offshore Standards DNV-OS-J101*, Section 3 – B 406 September 2011. http://www.dnv.com

Goda, Y. 1985. 'Random Seas and Design of Maritime Structures', 1st ed. p44. University of Tokio Press.

Hasager, C. B., Nielsen, N. M., Christiansen, M. B., Barthelmie, R. J., Astrup, P., 2007.' Advances on wind energy resource mapping from SAR'. *Advances in SAR Oceanography from Envisat and ERS Missions. Proceedings.* ed. / H. Lacoste. Paris: European Space Agency. (ESA-SP-613).

Lange, B., Larsen, S.E., Højstrup, J., & Barthelmie, R., 2002, 'Modelling the vertical wind speed and turbulence intensity profiles at prospective offshore wind farm sites', *1st WindWorld conference, Berlin, Germany*, 01-05-02.

Millar, D.L.; Smith, H.C.M., and Reeve, D.E., 2007. 'Modelling analysis of the sensitivity of shoreline changes to a wave farm'. *Ocean Engineering*, 34, 884–901.

NOAA National Geophysical Data Center, U.S. Coastal Relief Model, *Vol. 5.* http://www.ngdc.noaa.gov/mgg/coastal/crm.html

TELEMAC system. http://opentelemac.org

United Kingdom Hydrographic Office,'Admiralty Tide Tables Volume 2 – Europe (excluding United Kingdom and Ireland), Mediterranean Sea and Atlantic Ocean', 2011, p. 270